
Thermodynamics and Kinetics in the Synthesis of Monodisperse Nanoparticles

Nong-Moon Hwang, Jae-Soo Jung and Dong-Kwon Lee

Additional information is available at the end of the chapter

<http://dx.doi.org/10.5772/50324>

1. Introduction

The preparation of monodisperse nanoparticles with uniform size, shape and composition has been intensively pursued because of their scientific and technological interests [1-4]. The major advantage of monodisperse particles may be attributed to the uniform properties of individual particles, which makes the property of whole particles strictly controllable. They have been widely used in industries such as pharmacy, catalysts, sensors, film precursors, and information storage. The property of nanoparticles is much more sensitive to their size than that of micro-particles. For example, the fluorescence of monodisperse CdSe/ZnS core/shell nanoparticles depends strongly on their size [5]. The superparamagnetism also depends strongly on the size of nanoparticles [6]. The properties of these particular size nanoparticles show great potentials in the field of bio-medicals and electronics.

In general, to prepare the monodisperse nanoparticles in solution, the size had to be selected after somewhat polydisperse nanoparticles were produced. The separation procedures are very laborious and expensive because the size of nanoparticles is too small to be sorted. Moreover, the production yield of monodisperse nanoparticles decreases markedly due to the loss of nanoparticles during the separation procedures. Therefore, many efforts have been made to synthesize directly monodisperse nanoparticles without size selection procedures.

Recently, several methods have been developed successfully to synthesize gram quantity monodisperse nanoparticles directly without size selection procedures. One of them is a slow heating method developed by Hyeon et al. [6,7], which utilizes the burst nucleation followed by sustained growth of particles. Although nanoparticles have some size distribution in the nucleation stage, they became gradually monodisperse during growth. In this case, the principle for the direct synthesis of monodisperse nanoparticles could be approached by sustained growth of nuclei formed by burst nucleation with some initial size distribution [8].

The digestive ripening developed by Klabunde et al. [9-12] is another fascinating method for the direct synthesis of monodisperse nanoparticles. During digestive ripening, nanoparticles initially ranging from 2 to 40 nm were spontaneously transformed into particles with nearly uniform sizes of 4-5 nm. Lee et al. [13,14] could explain the digestive ripening process by considering the charge effect in the Gibbs-Thomson equation.

The purpose of this article is to provide the thermodynamic and kinetic basis to 'slow heating' method and digestive ripening, which are two successful processes to synthesize the monodisperse nanoparticles.

2. Evolution mechanism of monodisperse particles

To understand intuitively the underlying principle for the evolution of monodispersed particles, let's compare the growth of two spherical particles of different diameters of 1 nm and 5 nm as shown in Fig. 1(a). The problem could be simple under the assumption that all the particles grow at the same rate regardless of the size, which is valid for interface-controlled growth. The size ratio of two particles is 5, which is far from the monodisperse state. If the two particles grow by 1 nm after some time, their diameters become 2 nm and 6 nm, respectively, as shown in Fig. 1(b). Now the size ratio of the two particles is 3. If the two initial particles grow by 99 nm after an appreciable amount of time, their diameters become 100 nm and 104 nm, respectively, as shown in Fig. 1(c). Now their size ratio is 1.04, which is in the monodisperse state with the size being within 5% difference. The time evolution of the two particles in Fig. 1(a)-(c) shows that just the growth induces the monodispersity. It should be noted that the initial size difference between the two particles, which is 4 nm, is maintained throughout the growth but the size ratio continues to decrease with growth, approaching unity. This tendency to approach the monodisperse distribution by growth is often called 'focusing effect' [15].

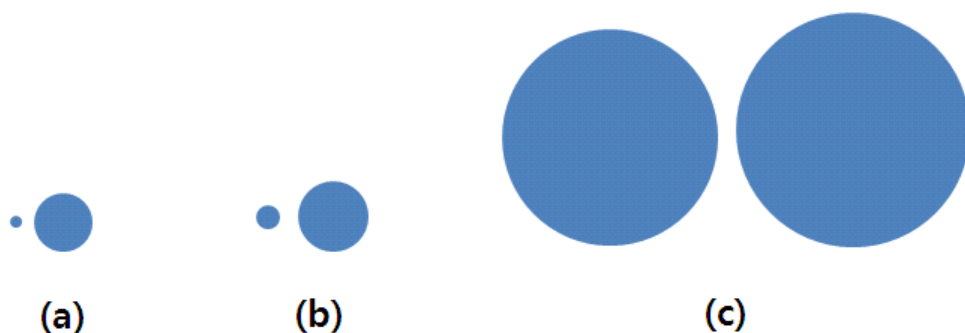


Figure 1. Initially, two spherical particles have the diameters of (a) 1 nm and 5 nm with the size ratio of 5. After growth by 1 nm, the respective particle becomes (b) 2 nm and 6 nm with the size ratio of 3. After growth by 99 nm, the respective particle becomes (c) 100 nm and 104 nm with the size ratio of 1.04, which has the monodispersity with size difference less than 5%.

If a colloidal particle grows in supersaturated solution, the solute may diffuse from the bulk liquid phase containing a uniform concentration of solute C_b to the particle surface through a diffusion layer with some concentration gradient where C_r is the solubility of the particle. In this condition the growth rate is described by

$$\frac{dr}{dt} = \frac{\frac{D}{r} \left(I + \frac{r}{\delta} \right) V_m (C_b - C_r)}{I + \frac{D}{kr} \left(I + \frac{r}{\delta} \right)} \quad (1)$$

where D is the diffusion coefficient of the solute, r is the particle radius, δ is the diffusion radius around a particle and k is the rate constant of the interface reaction of a solute at the particle interface.

If D is much larger than kr ($D \gg kr$), the interface reaction process becomes a rate-determining step and Eq. (1) is reduced to

$$\frac{dr}{dt} = kV_m (C_b - C_r) \quad (2)$$

In this case of the interface-controlled growth, the growth rate does not depend on the particle size. If D is much smaller than kr ($D \ll kr$), however, the diffusion process of a solute becomes a rate-determining step and thus Eq. (1) is reduced to

$$\frac{dr}{dt} = \frac{DV_m}{r} (C_b - C_r) \quad (3)$$

In this case of the diffusion-controlled growth, the growth rate is inversely proportional to the radius of each particle. This means that large particles grow more slowly than small ones, which is in contrast with the interface-controlled growth, where the growth rate was the same regardless of the size. Therefore, the diffusion-controlled growth has a stronger tendency to approach the monodisperse distribution than the interface-controlled growth.

The narrowing of the size distribution was first theoretically studied in the diffusion-controlled process by Reiss [16]. The variation of the radius distribution σ^2 during growth changes with time as follows.

$$\frac{d(\sigma^2)}{dt} = 2DV_m (C_b - C_r) \left[I - \bar{r} \overline{\left(\frac{1}{r} \right)} \right] \quad (4)$$

In Eq. (4), \bar{r} and $\overline{(1/r)}$ are the mean values of r and $1/r$, respectively. Since the arithmetic mean is larger than the harmonic mean, $\overline{(1/r)}$ is greater than $1/\bar{r}$. Therefore, in the supersaturated state, where $C_b > C_r$, Eq. (4) is negative. This means that the variation of the radius distribution σ^2 decreases with time as the growth continues.

3. Interface-controlled growth

The tendency to approach the monodisperse distribution by growth can be examined by computer simulation. Consider the case of interface-controlled growth. As a starting condition of simulation, it could be assumed that the number of particles is 1000 with the average size of 0.5 nm and particles have a spherical shape. It can also be assumed that the size distribution follows the Gaussian function. Since the Gaussian distribution spreads infinitely, the size distribution is cut off when its probability is less than 0.01. The width of the Gaussian distribution, which is defined as the difference between the maximum and minimum size with the probability of 0.01, was 2 nm. The center of the distribution was 0.5 nm. The radius ratio of the largest to the average-size particle was used as a criterion for the monodispersity. If this ratio is less than 1.05, the size distribution is regarded as being monodisperse. In the simulation, the growth rate, which is the same for all particles, was arbitrarily chosen to be 0.025 nm/s. It can further be assumed that there is no additional nucleation during growth, no coagulation between particles and no Ostwald ripening among particles.

Figs. 2 (a)-(c) show the particle size distribution, respectively, after 0 sec, 100 sec and 800 sec of growth. For visual representation of the result, the three-dimensional particles are projected on the two-dimensional plane. The location of the particles was randomly chosen within the square of the designated area but overlapping between particles was avoided. The broad size distribution in the initial state becomes narrower with particle growth, finally being monodisperse after 800 sec. The initial size ratio of 2.70 was decreased to 1.05 after the particle grew from the initial average radius of 0.5 nm to 21.49 nm. It should be noted that the broad size distribution in the initial state would be changed to the monodisperse state as far as the average size of particles grows from 0.5 nm to 21.49 nm regardless of the growth rate. Additional simulation was performed with the initial average radii of 1 nm and 2 nm. The final average particle radii reaching the monodisperse state were 41.18 nm and 81.02 nm, respectively.

These results can explain the natural evolution of monodisperse distribution of particles with growth. However, the results indicate that the minimum average radius for the monodisperse distribution should be about 20 nm when starting from the average radius of 0.5 nm, which is implicitly assumed to be the critical nucleus size. In the direct synthesis of monodisperse nanoparticles such as iron oxide reported by Hyeon et al. [6], however, the average radius is often as small as 4 nm. The average particle size to reach the monodisperse state shown in Fig. 2 is much larger than that observed experimentally in the direct synthesis of monodisperse nanoparticles.

Therefore, although the interface-controlled growth can explain the monodisperse evolution for particles larger than at least a few tens of nanometers, it cannot explain the evolution of monodisperse nanoparticles less than 10 nm, which requires that the monodisperse state should be reached at a much smaller particle size than that predicted by the interface-controlled growth. On the other hand, in the diffusion-controlled growth, the growth rate is inversely proportional to the particle radius as described by Eq. (3). Therefore, smaller particles would grow faster than larger ones, whose condition is more favorable in reaching the monodisperse state at smaller particle size. For this reason, the diffusion-controlled growth might be more suitable in explaining the evolution of the monodisperse nanoparticles less than 10 nm.

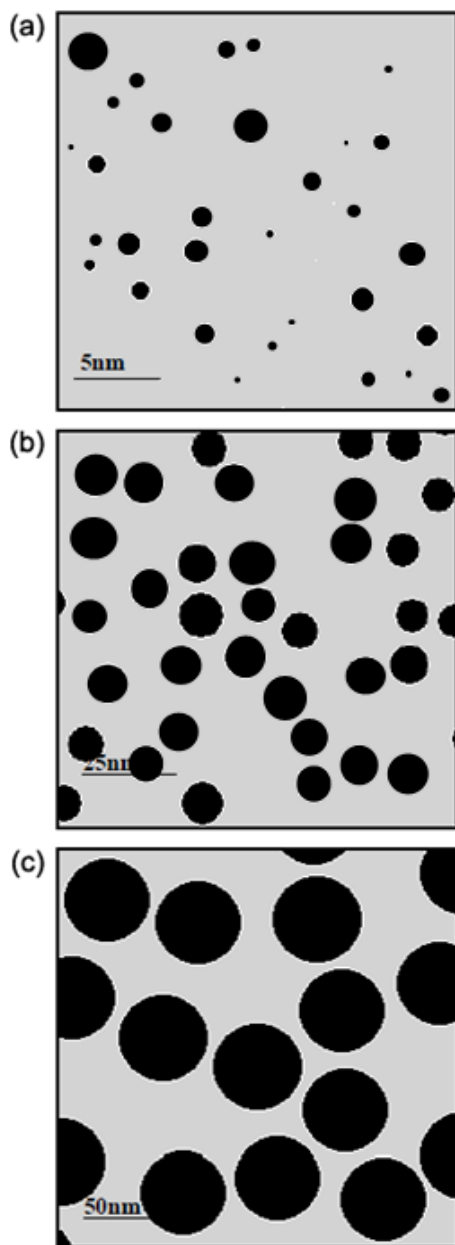


Figure 2. The numerical analysis of the particle growth under the condition of interface-controlled growth. (a) The initial size distribution: the average radius of the initial particles was set to 0.5 nm with 1 nm width between the maximum and average size. (b) The size distribution of particles in the intermediate stage after 100 s. (c) The monodisperse state evolved after 800 s with the average particle radius of 21.49 nm.

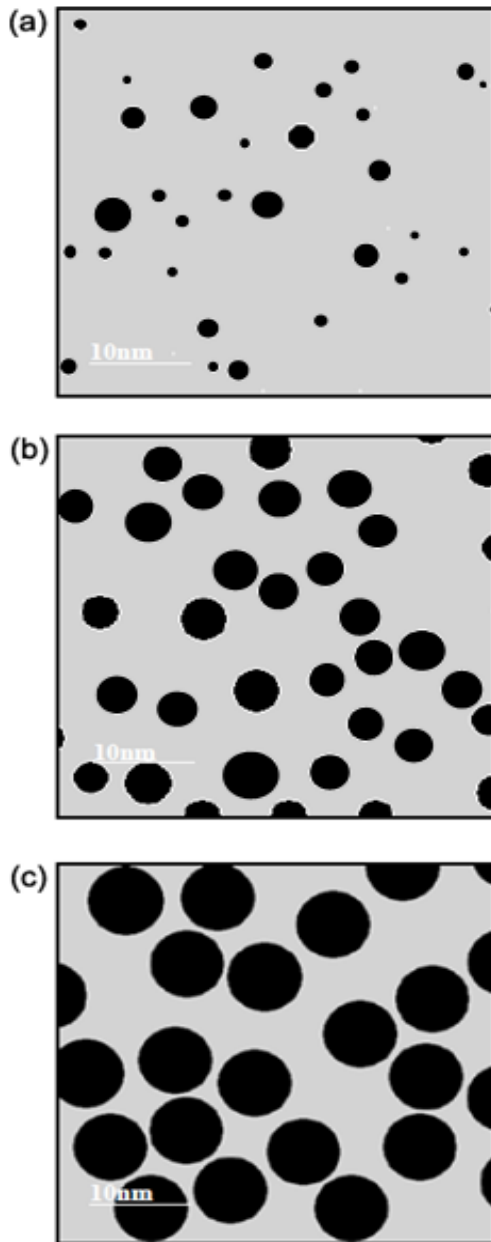


Figure 3. The numerical analysis of the particle growth under the condition of diffusion-controlled growth. (a) The initial size distribution: the average radius of particles was set to 0.5 nm with 1 nm width between maximum and average size. (b) The size distribution of particles in the intermediate stage after 100 s. (c) The monodisperse state evolved after 1200 s with the average particle radius of 4.5 nm.

4. Diffusion-controlled growth

The diffusion-controlled growth could also be investigated using the computer simulation. The initial particle size distribution was identical to the previous case: the average radius of 0.5 nm and the width of 2 nm for Gauss distribution. The time step for calculation was 1 sec. The concentration gradient was given a constant value of 0.75 mol/cm³ without the Gibbs-Thompson effect being considered, which results in removing the Ostwald ripening effect.

Figs. 3(a)-(c) show the two-dimensional display of particles, respectively, after 0 sec, 100 sec and 1200 sec by diffusion-controlled growth. The initial ratio of 2.70 was decreased to 1.05 after the particle grew from the initial average radius of 0.5 nm to 4.50 nm. It should be noted that the initial particle size distribution would become monodisperse with the size ratio of 1.05 as far as the average radius of the particles increases from 0.5 nm to 4.5 nm regardless of the growth rate if the growth is controlled by diffusion.

Comparison between Figs. 2 and 3 indicates that the monodisperse state is reached much faster and in a much smaller particle size by the diffusion-controlled growth than by the interface-controlled growth. Therefore, the direct synthesis of monodisperse nanoparticles by Hyeon et al. [6] can be explained by the diffusion-controlled growth. The present analysis indicates that even if there is a broad size distribution in the nucleation stage, it becomes narrower with growth, eventually leading to a monodisperse state. Because of this 'focusing effect', the evolution of the monodisperse nanoparticles seems to be a rule rather than an exception. Then, a question arises as to why people have difficulty in producing the monodisperse nanoparticles. Which factor would be critical in the successful synthesis of highly monodisperse nanoparticles?

5. Factors unfavorable for monodisperse distribution

There are factors which are unfavorable for monodispersity. These are additional nucleation, random coagulation and Ostwald ripening. It is well established that coagulation among particles can be inhibited by a suitable choice of surfactants. Therefore, coagulation is not a critical factor. The effect of Ostwald ripening becomes significant when the supersaturation is small. More precisely, if the supersaturation made by the capillarity or the Gibbs-Thompson effect of particles is higher than the supersaturation for growth in the bulk, Ostward ripening would occur extensively. Then, the size distribution would deviate from monodispersity and approach the well-established distribution predicted by the Lifshitz, Slyozov and Wagner (LSW) theory. [17, 18] Therefore, to inhibit Ostwald ripening, the supersaturation for growth should be maintained much higher than that by the Gibbs-Thompson effect. This aspect was studied in detail by Kwon et al. [8].

The most critical factor unfavorable for monodisperse distribution is the additional nucleation during growth. Therefore, growth should be separated from nucleation. The thermodynamics and kinetics of nucleation are relatively well established. The rate of

nucleation is negligibly low at low supersaturation and becomes very high above certain supersaturation, varying like a step function. The supersaturation for the onset of nucleation has a special meaning and is called 'the critical supersaturation for nucleation', which is defined as the supersaturation to produce the nucleation rate of $1/\text{cm}^3\cdot\text{sec}$.

Consequently, to inhibit the additional nucleation during growth, the supersaturation should be maintained below the critical supersaturation for nucleation. Normally, the critical supersaturation for homogeneous nucleation is high enough but that for heterogeneous nucleation is relatively low and can be easily achieved. Therefore, a special care must be taken to prepare the reactor for the synthesis of monodisperse nanoparticles free from the site for heterogeneous nucleation.

One attempt to separate growth from nucleation is the seed-mediated growth, where the preformed nanoparticles are used as seed nuclei [7, 19]. Another attempt to separate growth from nucleation is the initial burst of nucleation, where an appreciable amount of supersaturation is consumed during the burst of nucleation and the relatively low supersaturation is maintained during growth. The 'hot-injection' method [20-22] is an example of this attempt.

Rapid injection of reagents into a hot surfactant solution raises the precursor concentration above the nucleation threshold. A burst of nucleation during a short period of time partially relieves the supersaturation. If the rate of the precursor consumption by the growing colloidal nanoparticles is not exceeded by the rate of precursor addition to solution, no new nuclei would form. This process typically produces the nanoparticles with the size distribution of $10 < \sigma < 15\%$ in diameter, which are then narrowed to $< 5\%$ through additional size-selective processing.

The 'heating-up' method [6, 23-25] is a new attempt to separate growth from nucleation. This process is a batch process and very simple. Metal-oleate precursors are prepared from metal chloride and sodium oleate. If the metal-oleate precursors are heated in a high-boiling point solvent, they are thermally decomposed and produce monodisperse nanocrystals. This method proved to be advantageous for large-scale production. Park et al. [6] showed that as large as 40g of monodisperse magnetite nanocrystals with a yield of $>95\%$ could be produced in a batch. The size uniformity of the nanoparticles is usually better than that by the 'hot-injection' method. Since this is a batch process, the precursors are not added during growth to supplement the supersaturation.

The supersaturation that has been consumed during growth can be indirectly estimated from the final size of the nanoparticles. The highly monodisperse nanoparticles were reported to grow as large as 22 nm in the 'heating up' process. Considering that the critical nucleus size is ~ 0.5 nm, the diameter increases by more than 20 nm, which implies that a considerable supersaturation must have been consumed. Since an appreciable amount of supersaturation is consumed in the initial nucleation process, the remaining supersaturation is usually not so high. Therefore, it is highly unlikely that the nuclei should grow as large as

10 nm by remaining supersaturation without precursors being supplied additionally. It should be reminded that in the 'hot-injection' method the additional precursors should be supplied to produce nanoparticles larger than 10 nm.

Then, a question arises as to why additional nucleation does not occur during such extensive growth. It appears that all the supersaturation, which should be consumed to produce the final size of nanoparticles, is not built up simultaneously but only a very small fraction of supersaturation, which is too small to trigger the nucleation, is maintained throughout the growth. This is an ideal situation where growth is separated from nucleation. One possibility to realize such an ideal situation is that the decomposition of the metal orleate complex into metal does not occur in the solution but occurs only at the surface of nanoparticles. In other words, the surface of nanoparticles acts as the catalytic site for decomposition of the metal orleate. This type of reaction is called 'self-catalytic'. Therefore, if a system is self catalytic, growth can be separated ideally from nucleation and monodisperse nanoparticles can be easily synthesized.

6. Digestive ripening

As mentioned earlier, the coarsening kinetics of Ostwald ripening has been well established by LSW theory [17, 18]. During Ostwald ripening, large particles with a low chemical potential grow at the expense of small particles with a high chemical potential and, as a consequence, the average size increases and the total number of particles decreases during coarsening. Eventually, only one large particle remains, which corresponds to a final equilibrium state.

However, Klabunde and co-workers reported a series of articles on the synthesis of monodisperse gold or silver nanocrystals by a digestive-ripening process of polydisperse nanocrystals. [9-12, 26, 27] Gram quantities of monodisperse gold or silver nanoparticles could be produced through digestive ripening, where colloidal particles from 2 to 40 nm are transformed to nearly monodisperse particles of 4–5 nm diameters.

Digestive ripening is the reverse process of Ostwald ripening. It is interesting and also puzzling in that small particles grow at the expense of large ones. Clearly, digestive ripening cannot be understood with the usual Gibbs–Thomson equation solely based on a curvature effect. According to the theory of diffusion-controlled coarsening [28], the growth rate of a particle with radius, r , is given by

$$\frac{dr}{dt} = \frac{D_f V_g C_o}{rRT} [\mu(r)^* - \mu(r)] \quad (5)$$

where R is the gas constant, T the absolute temperature, and D_f and C_o are the diffusivity and solubility of atoms in the solution, respectively. Eq. (5) is valid when the diffusion field does not overlap. $\mu(r)^*$ is the chemical potential of a particle of critical size, which neither grows nor shrinks at the given instant.

Since the phenomenon of digestive ripening runs counter to the decrease of interfacial free energy, a different type of free energy must be involved. The driving force for digestive ripening must compete against the reduction of the interface free energy. There are two such free energies. One is strain energy and the other is electrostatic energy. Since solid particles dispersed in liquid do not have any appreciable strain energy, the electrostatic energy is a possible candidate. In fact, Klabunde et al, who have developed the digestive ripening process, reported that their nanoparticles were negatively charged [9, 10]. If nanoparticles are electrically charged, they have an electrostatic energy inversely proportional to the radius of the particles. Since electrostatic energy increases with decreasing particle size, charged particles cannot shrink away completely. Therefore, the presence of charge can drastically change the Ostwald ripening behavior. The chemical potential change arising from the presence of charge can be treated by modifying the Gibbs-Thomson equation in consideration of the electrostatic energy.

To analyze the effect of charge on the coarsening behavior of nanoparticles, it is assumed that each particle is singly charged, electrically-conducting, and spherical with isotropic interface free energy, dispersed in a matrix phase with a dielectric constant of 1. According to this assumption, ions are regarded as the primary embryos of charged nanoparticles. It is further assumed that the charged nanoparticles do not coagulate with each other and that the atomic transfer between particles is diffusion-controlled. The Gibbs free energy of a spherical conducting particle with radius r and charge e (corresponding to the unit charge of an electron) is expressed as

$$\Delta G = 4\pi r^2 \sigma + k \frac{e^2}{2r}, \quad (6)$$

where σ is the interface free energy of the particle and k is defined by $1/(4\pi\epsilon)$, where ϵ is the vacuum permittivity [29]. ke^2 is 2.3068×10^{-28} N·m². It should be noted that with decreasing r , the interface free energy term decreases but the electrostatic energy term increases.

From Eq. (6), the modified Gibbs-Thomson equation is derived as

$$\Delta\mu = \mu_r - \mu_o = RT \ln \frac{C_r}{C_o} = V_m \left(\frac{2\sigma}{r} - k \frac{q^2}{8\pi r^4} \right), \quad (7)$$

where C_o is the solute concentration in the matrix without capillary effect. If the difference between C_r and C_o is small, the equation can be approximated as

$$\ln \left(\frac{C_r}{C_o} \right) \approx \frac{C_r - C_o}{C_o} = \frac{V_m}{RT} \left(\frac{2\sigma}{r} - k \frac{q^2}{8\pi r^4} \right). \quad (8)$$

The coarsening behavior can be analyzed quantitatively by solving Eqs. (5) and (8) simultaneously under the constraint of mass conservation for a total number of particles N_p , and is expressed as

$$\sum_n^{N_p} 4\pi r_n^2 \frac{dr_n}{dt} = 0. \quad (9)$$

Substituting Eq. (5) into Eq. (9) yields

$$\sum_n^{N_p} r_n D_f V_m (C^* - C_0 - (C_{r,n} - C_0)) = 0. \quad (10)$$

From Eqs. (5), (9) and (10), the following equation can be derived:

$$\frac{dr_n}{dt} = \frac{D_f V_m^2 C_0}{RT r_n} \left(\sum_n^{N_p} \left(\frac{r_n}{\sum_n^{N_p} r_n} \left(\frac{2\sigma}{r_n} - k \frac{q^2}{8\pi r_n^4} \right) \right) - \left(\frac{2\sigma}{r_n} - k \frac{q^2}{8\pi r_n^4} \right) \right). \quad (11)$$

If the growth rate of each particle is determined by Eq. (11), the new radius after dt is given by

$$r_n(t + dt) = r_n(t) + \left(\frac{dr_n}{dt} \right) dt. \quad (12)$$

Once the initial size distribution of particles is given, the time-dependent size distribution can be obtained by solving equations (11) and (12) simultaneously by iteration.

To demonstrate that this approach reproduces simple digestive ripening, one large charged nanoparticle of 15 nm radius and 600 ions of 0.2 nm radius were chosen as an initial state. A diffusivity, D_i , of $10^{-9} \text{ m}^2\text{sec}^{-1}$ and a temperature of 393 K were chosen for calculation.[11] Besides, the interface energy of $\sigma = 1 \text{ mJ}\cdot\text{m}^{-2}$, $C_0 = 0.01 \text{ mol}\cdot\text{m}^{-3}$, and $V_m = 1.02 \times 10^{-5} \text{ m}^3 \cdot \text{mol}^{-1}$, which is the molar volume of gold, were chosen. Here, the interface free energy of $1 \text{ mJ}\cdot\text{m}^{-2}$ is chosen, simply because it produces monodisperse nanoparticles of the 1.5 ~ 2 nm size after digestive ripening. Experimentally, the surfactant, dodecanethiol, which is expected to diminish the interface free energy between gold and solution, appears to play a critical role in inducing digestive ripening. [30, 31] As the interface free energy decreases and the electric charge density increases, the size of finally-evolved monodisperse nanoparticles increases.

Fig. 4 shows the size evolution of charged nanoparticles with time. a1 and a2 in Fig. 4(a) represent the radius of charged embryos at 200 s and 600 s, respectively. Likewise, b1 and b2 in Fig. 4(a) represent the radius of the 15 nm particle at 200 sec and 600 sec, respectively. The size of the small charged embryos increases, whereas the size of the large charged particles decreases. Figs 4(b)-(d) show a display of the size distribution of nanoparticles at 200 s, 600 s and 900 s, respectively. Finally, the radius of every nanoparticle becomes 1.78 nm at 900 s, as shown in Fig. 4(d), which corresponds to 'F' in Fig. 4(a), producing perfect monodisperse

nanoparticles. This calculation reproduces the experimentally observed digestive ripening behavior.

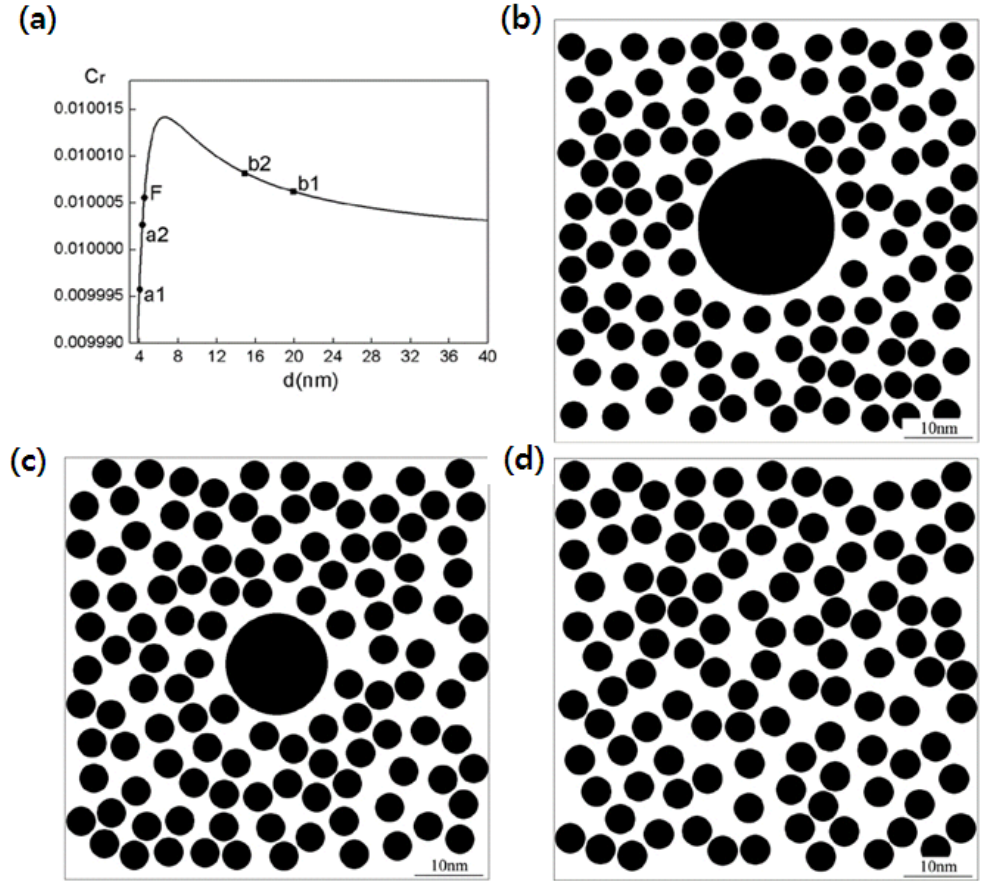


Figure 4. Coarsening behavior of one big particle of 30 nm and 300 embryos of 0.4 nm. (a) a1 and a2 indicate the size of embryos at 200 s and 500 s, respectively. Likewise b1 and b2 indicate the size of the large nanoparticle at 200 s and 500 s, respectively. Finally, the size of every nanoparticle becomes the same on F at 900s. The size distribution of nanoparticles at (b) 200 s, (c) 500 s and (d) 900 s, respectively. In (b), the size of small nanoparticles is 4 nm and that of a large nanoparticle is 19.9 nm. In (c), the size of small nanoparticles is 4.3 nm and that of a large nanoparticle is 14.9 nm. In (d), the size of every nanoparticle becomes 4.5 nm. Reprinted with permission from [13]. Copyright 2007 Elsevier.

7. Digestive ripening in a binary system

Smetana et al. [26] reported digestive ripening in a binary system, where separately prepared monodisperse Au and Ag nanoparticles with a radius of ~3.3 nm, mixed in a colloid solution, were transformed into monodisperse Au/Ag alloy nanoparticles with a radius of ~2.8 nm. The final monodisperse nanoparticles did not have a core-shell structure but had uniform composition distribution. The size of the final monodisperse nanoparticles was reduced in comparison to that of the initial unalloyed monodisperse nanoparticles, which implied that additional nucleation had occurred during digestive ripening.

To analyze the coarsening behavior of a binary system of Au and Ag nanoparticles, the chemical potential of a binary system needs to be derived. According to the phase diagram of an Au/Ag binary system [31], Au and Ag, which have the same face-centered cubic (FCC) structure and a small difference in atomic size, have a complete solid solution. Therefore, it is assumed that Au and Ag nanoparticles behave like an ideal binary solid solution, and then, the Gibbs-free energy is expressed in the whole composition range as follows [32]:

$$G = X_{Au}G_{Au} + X_{Ag}G_{Ag} + RT(X_{Au}\ln X_{Au} + X_{Ag}\ln X_{Ag}) \quad (13)$$

From Eq. (13), the chemical potentials of Au and Ag for the alloy are given, respectively, by

$$\begin{aligned} \mu_{Au} &= G_{Au} + RT\ln X_{Au} \\ \mu_{Ag} &= G_{Ag} + RT\ln X_{Ag} \end{aligned} \quad (14)$$

where G_{Au} and G_{Ag} are the molar free energies of pure Au and Ag, respectively; and X_{Au} and X_{Ag} are the mole fractions of Au and Ag, respectively. From Eqs. (7) and (14), the chemical potentials of spherically charged nanoparticles of Au and Ag with radius r can be derived as

$$\begin{aligned} \mu_{Au}(r) &= G_{Au} + RT\ln X_{Au} + V_{SS} \left[\frac{2\sigma_{SS}}{r} - \frac{kz^2q^2}{8\pi r^4} \right] \\ \mu_{Ag}(r) &= G_{Ag} + RT\ln X_{Ag} + V_{SS} \left[\frac{2\sigma_{SS}}{r} - \frac{kz^2q^2}{8\pi r^4} \right] \end{aligned} \quad (15)$$

where σ_{SS} and V_{SS} are the interface free energy and the molar volume of the Au/Ag solid solution, respectively. To investigate the time evolution of the coarsening behavior of the mixed Au and Ag nanoparticles, the growth rate of particles should be calculated.

Substituting Eq. (5) for dr/dt in Eq. (9) and rearranging the result yield

$$\mu(r)^* = \left[\sum_{n=1}^{N_p} r_n \mu(r_n) \right] / \sum_{n=1}^{N_p} r_n \quad (16)$$

Expressing $\mu(r)^*$ in terms of dr_i/dt and using Eq. (15) for $\mu(r)$ in Eq. (16), the growth rate of the i th particle by diffusion of Au and Ag atoms is obtained as

$$\frac{dr_i}{dt} = \frac{D_f V_{SS}^2 C_o}{r_i RT} \left\{ -\frac{RT}{V_{SS}} \ln X_{Au} - \frac{2\sigma_{SS}}{r_i} + \frac{kz^2 q^2}{8\pi r_i^4} + \left(\sum_{n=1}^{N_p} r_n \right)^{-1} \sum_{n=1}^{N_p} r_n \left[\frac{RT}{V_{SS}} \ln X_{Au} + \frac{2\sigma_{SS}}{r_n} - \frac{kz^2 q^2}{8\pi r_n^4} \right] \right\},$$

$i = 1, 2, \dots$ for Au

$$\frac{dr_i}{dt} = \frac{D_f V_{SS}^2 C_o}{r_i RT} \left\{ -\frac{RT}{V_{SS}} \ln X_{Ag} - \frac{2\sigma_{SS}}{r_i} + \frac{kz^2 q^2}{8\pi r_i^4} + \left(\sum_{n=1}^{N_p} r_n \right)^{-1} \sum_{n=1}^{N_p} r_n \left[\frac{RT}{V_{SS}} \ln X_{Ag} + \frac{2\sigma_{SS}}{r_n} - \frac{kz^2 q^2}{8\pi r_n^4} \right] \right\},$$

$i = 1, 2, \dots$ for Ag

(17)

With Eq. (17), the radius of the i th particle can be calculated at a time, $t + \Delta t$, by

$$r_i(t + \Delta t) = r_i(t) + \frac{dr_i}{dt} \Delta t, \quad i = 1, 2, \dots \quad (18)$$

The analytic expression for the composition change of nanoparticles cannot be derived. Therefore, the composition change of nanoparticles should be computed from the mass change of each element, which is determined from the size change by Eq. (18) for each iteration.

To check whether these schemes reproduce the experimental result of alloy digestive ripening, a simple system of 500 Au charged nanoparticles of $R_{Au} = 3.3$ nm, 500 Ag charged nanoparticles of $R_{Ag} = 3.3$ nm and 500 charged nuclei of $R_{nuclei} = 0.5$ nm was considered. This system is chosen to represent the experimental condition of as-prepared Au and Ag nanoparticles mixed for digestive ripening [14]. The 500 nuclei were added because the experimental fact that the number of final nanoparticles increases after digestive ripening indicates that additional nucleation occurs. The capital letter R_i indicates an initial radius with the suffix i implying the i th group of particles with identical radius. The initial mole fraction of Au nanoparticles, X_{Au} , is set at 0.99 instead of 1 to avoid the infinity in calculation. In the same manner, X_{Au} of Ag nanoparticles and the size of nuclei are set at 0.01 and 0.5, respectively. The parameters used are $D_f = 0.5 \times 10^{-14}$ m²/s, $V_{SS} = 1.02 \times 10^{-5}$ m³/mol, $C_o = 0.01$ mol/m³, $kq^2 = 2.3068 \times 10^{-28}$ J·m, $T = 393$ K, $\sigma_{SS} = 0.3$ J/m², and $z = 30$. It should be noted that if the particles are assumed to be singly charged with $z = 1$, the interface energy σ_{SS} should have a much smaller value than 0.3 J/m² to reproduce the experimentally-observed digestive ripening.

For the simplification, the diffusivities of Au or Ag atoms in the nanoparticles are assumed to be high enough to be homogenized immediately because the final structure of Au/Ag alloy nanoparticles was reported not to have a core-shell structure but to have a homogeneous solid solution.

In Fig. 5, the coarsening behavior of nanoparticles with time is schematically displayed. The time evolution of the microstructure is shown in Figs. 5(a), (b), (c) and (d) at $t_1 = 0$, $t_2 = 1$, $t_3 = 2$ and $t_4 = 16$ h, respectively. Fig. 5(a) shows the initial size distribution and the composition

of nanoparticles, which is represented by the gray scale from black for Au to white for Ag as shown by the gray scale bar in Fig. 5. Therefore, black, white and gray nanoparticles represent Au-rich, Ag-rich and Au/Ag alloy nanoparticles, respectively. After 1 h, the radii of both Au and Ag nanoparticles decrease to 3.07 nm and the mole fractions, X_{Au} , of Au and

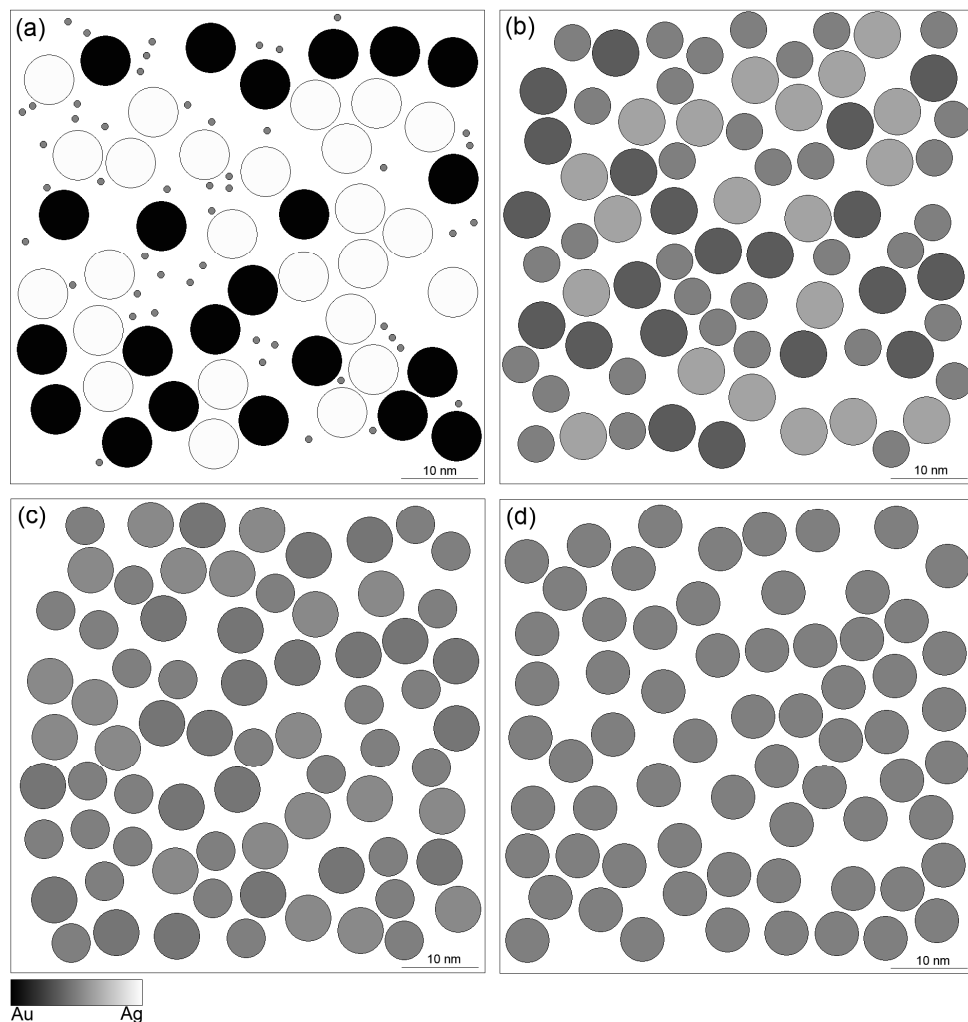


Figure 5. Display of the nanoparticles evolved through coarsening at four different times in the system of 500 Au nanoparticles, 500 Ag nanoparticles and 500 nuclei. Composition is represented by the gray scale from Au as black to Ag as white. (a) At $t_1 = 0$ h, $R_{Au} = 3.3$ nm with $X_{Au} = 0.99$, $R_{Ag} = 3.3$ nm with $X_{Au} = 0.01$ and $R_{nuclei} = 0.5$ nm with $X_{Au} = 0.5$. (b) At $t_2 = 1$ h, $r_{Au} = 3.07$ nm with $X_{Au} = 0.64$, $r_{Ag} = 3.07$ nm with $X_{Au} = 0.36$ and $r_{nuclei} = 2.4$ nm with $X_{Au} = 0.5$. (c) At $t_3 = 2$ h, $r_{Au} = 3$ nm with $X_{Au} = 0.54$, $r_{Ag} = 3$ nm with $X_{Au} = 0.46$ and $r_{nuclei} = 2.6$ nm with $X_{Au} = 0.5$. (d) At $t_4 = 16$ h, all the particles become monodisperse at 2.88 nm with the same composition of $X_{Au} = 0.5$. Reprinted with permission from [14]. Copyright 2009 Elsevier.

Ag nanoparticles become 0.64 and 0.36, respectively, as shown in Fig. 5(b). The radii of the nuclei increase to 2.4 nm with their mole fraction, X_{Au} , maintained as 0.5. After 2 h, the size distribution becomes much narrower approaching a monodisperse state and the composition becomes more homogenized as shown in Fig. 5(c). The radii of initial Au and Ag nanoparticles decrease to 3 nm, and the radii of the nuclei increase to 2.6 nm. The mole fractions of Au and Ag nanoparticles become 0.54 and 0.46, respectively. After 16 h, all the nanoparticles eventually have the same radius of 2.88 nm and the same composition of $X_{\text{Au}} = 0.5$, as shown in Fig. 5(d). By considering both the electrostatic energy and ideal solid solution, the coarsening behavior of the digestive ripening process, where the separated Au and Ag nanoparticles were transformed into monodisperse Au/Ag alloy nanoparticles, was successfully reproduced.

8. Conclusions

The evolution mechanism of monodisperse nanoparticles is approached thermodynamically and kinetically. Both interface-controlled and diffusion-controlled growth of particles can induce monodisperse distribution of particles if coagulation, additional nucleation and Ostwald ripening are inhibited. The diffusion-controlled growth reaches the monodisperse state at much smaller size than the interface-controlled growth. The evolution mechanism of monodisperse nanoparticles by digestive ripening is approached using the modified Gibbs-Thompson equation considering electrostatic energy. The digestive ripening behavior of both pure metal and alloy which is contrary to conventional Ostwald ripening, is well explained assuming that nanoparticles are electrically charged.

Author details

Nong-Moon Hwang and Jae-Soo Jung

Department of Materials Science and Engineering, Seoul National University, Seoul, Korea

Dong-Kwon Lee

LG Chem. Ltd, Research Park, Yoseong-gu, Daejeon, Korea

Acknowledgement

This work was supported by the National Research Foundation of Korea (NRF) grant funded by the Korea government (MEST) (No. M10600000159-06J0000-15910).

9. References

- [1] K. J. Klabunde, *Nanoscale Materials in Chemistry*, (Wiley-Interscience, New York, 2001).
- [2] T. Sugimoto, *Monodispersed Particles*, (Elsevier, Amsterdam, 2001).
- [3] G. Schmid, *Nanoparticles: From Theory to Application*, (WILEY-VCH, Weinheim, 2004).

- [4] J. N. Park, S. G. Kwon, J. Joo, Y. G. Jang, and T. H. Hyeon, *Angew. Chem. Int.*, **46**, 4630 (2007).
- [5] I. L. Medintz, H. T. Uyeda, E. R. Goldman, and H. Mattoussi, *Nature Mater.*, **4**, 435 (2005).
- [6] J. N. Park, K. J. An, Y. S. Hwang, J. G. Park, H. J. Noh, J. Y. Kim, J. H. Park, N. M. Hwang, and T. H. Hyeon, *Nature Mater.*, **3**, 891 (2004).
- [7] J. N. Park, E. W. Lee, N. M. Hwang, M. S. Kang, S. C. Kim, Y. S. Hwang, J. G. Park, H. J. Noh, J. Y. Kim, J. H. Park, and T. H. Hyeon, *Angew. Chem. Int.*, **44**, 2872 (2005).
- [8] S. G. Kwon, Y. Piao, J. N. Park, S. Angappane, Y. G. Jo, N. M. Hwang, J. G. Park, and T. H. Hyeon, *J. Am. Chem. Soc.*, **129**, 12571 (2007).
- [9] G. Trivino, K. J. Klabunde, and E. Dale, *Langmuir*, **3**, 986 (1987).
- [10] B. L. V. Prasad, S. I. Stoeva, C. M. Sorensen, and K. J. Klabunde, *Langmuir*, **18**, 7515 (2002).
- [11] S. Stoeva, K. J. Klabunde, C. Sorensen, and I. Dragieva, *J. Am. Chem. Soc.*, **124**, 2305 (2002).
- [12] B. L. V. Prasad, S. I. Stoeva, C. M. Sorensen, and K. J. Klabunde, *Chem. Mater.*, **15**, 935 (2003).
- [13] D. K. Lee, S. I. Park, J. K. Lee, and N. M. Hwang, *Acta Mater.*, **55**, 5281 (2007).
- [14] D. K. Lee and N. M. Hwang, *Scripta Mater.*, **61**, 304 (2009).
- [15] X. Peng, J. Wickham, A.P. Alivisatos, *J. Am. Chem. Soc.* **120**, 5343 (1998).
- [16] H. Reiss, *J. Chem. Phys.* **19**, 482 (1951).
- [17] I. M. Lifshitz, V. V. Slyozov, *J. Phys. Chem. Solids* **19**, 35 (1961).
- [18] C. Wagner, *Zeitschrift fuer Elektrochemie* **65**, 581 (1961)
- [19] N. R. Jana, L. Gearheart, C. J. Murphy, *Chem. Mater*, **12**, 2313 (2001), H. Yu, P.C. Gibbons, K. F. Kelton, W. E. Buhro, *J. Am Chem, Soc.* **123**, 9198 (2001).
- [20] C. B. Murray, D. J. Norris, M.G. Bawendi, *J. Am. Chem. Soc.*, **115**, 8706 (1993).
- [21] D. V. Talapin, A. L. Rogach, A. Kornowski, M. Haase, H. Weller, *Nano Lett.*, **1**, 207 (2001).
- [22] J. Hambrock, R. Becker, A. Birkner, J. Weiss, R. A. Fischer, *Chem. Commun.* **68** (2002), N.R. Jana, X. Peng, *J. Am. Chem. Soc.*, **125**, 14280 (2003).
- [23] W. S. Seo, H. H. Jo, K. Lee, J. T. Park, *Adv. Mater.*, **15**, 795 (2003).
- [24] W. W. Yu, J. C. Falkner, C. T. Yavuz, V.L. Colvin, *Chem. Commun.*, 2306 (2004).
- [25] J. Joo, H. B. Na, T. Yu, J. H. Yu, Y. W. Kim, F. Wu, J. Z. Ahang, T. Hyeon, *J. Am. Chem.Soc.*, **125**, 11100 (2003).
- [26] A. B. Smetana, K. J. Klabunde, C. M. Sorensen, A. A. Ponce, B. Mwale, *J. Phys. Chem. B*, **110**, 2155 (2006).
- [27] D. V. Leff, P. C. Ohara, J. R. Heath, W. M. Gelbart, *J. Phys. Chem.*, **99**, 7036 (1995).
- [28] P. G. Shewmon, *Transformations in Metals*, (McGraw-Hill, New York, 1969).
- [29] E. A. Boucher, *Nucleation* (ed. A. C. Zettlemoyer), (Marcel Dekker, INC, New York, 1969).
- [30] I. Stalder, *J. Chem. Phys.* **118**, 7981 (2003).

- [31] H. Okamoto, T. B. Massalski, Phase Diagrams of Binary Gold Alloys, (ASM International, Metals Park OH, 1987).
- [32] D. A. Porter, K. E. Easterling, Phase Transformations in Metals and Alloys, (Chapman & Hall, London, 1992).